









RESEARCH ARTICLE

Tumor Markers and Signatures

Histomic and transcriptomic features of MRI-visible and invisible clinically significant prostate cancers are associated with prognosis

Timo-Pekka K. Lehto^{1,2,3}  | Juho Pylväläinen⁴  | Kevin Sandeman⁵  |
 Anu Kenttämies⁴  | Stig Nordling¹  | Ian G. Mills^{6,7} | Jing Tang^{3,8}  |
 Tuomas Mirtti^{1,3,9,10}  | Antti Rannikko^{2,3,10} 

¹Department of Pathology, University of Helsinki and Helsinki University Hospital, Helsinki, Finland

²Department of Urology, University of Helsinki and Helsinki University Hospital, Helsinki, Finland

³Research Program in Systems Oncology, Faculty of Medicine, University of Helsinki, Helsinki, Finland

⁴Department of Radiology, University of Helsinki and Helsinki University Hospital, Helsinki, Finland

⁵Department of Pathology, Region Skåne, Malmö, Sweden

⁶Nuffield Department of Surgical Sciences, University of Oxford, Oxfordshire, UK

⁷Patrik G Johnston Centre for Cancer Research, Queen's University of Belfast, Belfast, UK

⁸Department of Biochemistry and Developmental Biology, University of Helsinki, Helsinki, Finland

⁹Department of Biomedical Engineering, School of Medicine, Emory University, Atlanta, Georgia, USA

¹⁰iCAN-Digital Precision Cancer Medicine Flagship, Helsinki, Finland

Correspondence

Timo-Pekka K. Lehto, Department of Urology, University of Helsinki, Haartmaninkatu 8, 00290, Helsinki, Finland.
 Email: timo-pekka.lehto@helsinki.fi

Abstract

Magnetic resonance imaging (MRI) is increasingly used to triage patients for prostate biopsy. However, 9% to 24% of clinically significant (cs) prostate cancers (PCas) are not visible in MRI. We aimed to identify histomic and transcriptomic determinants of MRI visibility and their association to metastasis, and PCa-specific death (PCSD). We studied 45 radical prostatectomy-treated patients with csPCa (grade group [GG]2-3), including 30 with MRI-visible and 15 with MRI-invisible lesions, and 18 men without PCa. First, histological composition was quantified. Next, transcriptomic profiling was performed using NanoString technology. MRI visibility-associated differentially expressed genes (DEGs) and Reactome pathways were identified. MRI visibility was classified using publicly available genes in MSK-IMPACT and Decipher, Oncotype DX, and Prolaris. Finally, DEGs and clinical parameters were used to classify metastasis and PCSD in an external cohort, which included 76 patients with metastatic GG2-4 PCa, and 84 baseline-matched controls without progression. Luminal area was lower in MRI-visible than invisible lesions and low luminal area was associated with short metastasis-free and PCa-specific survival. We identified 67 DEGs, eight of which were associated with survival. Cell division, inflammation and transcriptional regulation pathways were upregulated in MRI-visible csPCas. Genes in Decipher, Oncotype DX and MSK-IMPACT performed well in classifying MRI visibility (AUC = 0.86-0.94). DEGs improved classification of metastasis (AUC = 0.69) and PCSD (AUC = 0.68) over clinical parameters. Our data reveals that MRI-visible csPCas harbor more aggressive histomic and transcriptomic features than MRI-invisible csPCas. Thus, targeted

Abbreviations: ADC, apparent diffusion coefficient; cs, clinically significant; CSS, cancer-specific survival; DCE, dynamic contrast enhancement; DEG, differentially expressed gene; DWI, diffusion weighted imaging; FFPE, formalin-fixed paraffin-embedded; GG, grade group; HUS, Helsinki University Hospital; MFS, metastasis-free survival; MRI, multi-parametric magnetic resonance imaging; PCa, prostate cancer; PCSD, prostate cancer-specific death; PI-RADS, prostate imaging-reporting and data system; PSA, prostate-specific antigen; PSA-D, prostate-specific antigen density; RF, random forest; RP, radical prostatectomy; T2WI, T2 weighted image; TBx, targeted biopsies; TMA, tissue microarray; TSE, turbo-spin-echo.

This is an open access article under the terms of the [Creative Commons Attribution](https://creativecommons.org/licenses/by/4.0/) License, which permits use, distribution and reproduction in any medium, provided the original work is properly cited.

© 2023 The Authors. *International Journal of Cancer* published by John Wiley & Sons Ltd on behalf of UICC.

Funding information

Academy of Finland; Finnish State Research Funding; Jane ja Aatos Erkon Säätiö; Syöpäsäätiö

biopsy of visible lesions may be sufficient for risk stratification in patients with a positive MRI.

KEYWORDS

biomarker, decipher, MSK-IMPACT, Oncotype DX, Prolaris

What's new?

MRI-visible prostate cancers (PCa) were shown to histologically harbor lower luminal area than baseline-matched MRI-invisible PCas. On transcript level, MRI-visible and invisible PCas had differential gene expression. Both, low luminal area, and gene expression in MRI-visible PCas were associated with poor prognosis. Proliferation, inflammation and transcriptional regulation was upregulated in MRI-visible PCas. Prognostic panels were able to classify MRI-visibility. Targeted biopsy of visible lesions might be enough for accurate risk stratification of MRI-positive patients.

1 | INTRODUCTION

Prostate cancer (PCa) is the second most common cancer in men globally.¹ Guidelines recommend pre-biopsy multi-parametric magnetic resonance imaging (MRI) and targeted biopsies (TBx) with or without systematic biopsy.² PCas are histologically graded according to the International Society of Urological Pathology grade group (GG) system.³ Most men are diagnosed with GG2-4 PCa.

In 2012, the European Society of Urogenital Radiology published the Prostate Imaging-Reporting and Data System (PI-RADS),⁴ which was updated by the American College of Radiology in 2015⁵ and 2019.⁶ PI-RADS is a 5-tier assessment scale providing the probability of clinically significant PCa (csPCa).⁵ PI-RADS scores 0-2 are considered negative, that is, csPCa is unlikely, while scores 3-5 are considered positive and are associated with increasing likelihood of csPCa. csPCa is defined in PI-RADSv2 as \geq GG2 with lesion volume \geq 0.5 ml and/or extraprostatic extension.⁵ Of patients having PI-RADS 5 lesions, 65% to 80% have csPCa, while 9% and 24% of those with negative MRI have csPCa in biopsy or radical prostatectomy (RP) specimens.⁷⁻¹⁰ True biological and clinical significance of MRI-invisible lesions remains unclear as long-term follow-up data is missing.

PCa is typically multifocal.^{11,12} These foci are genetically heterogeneous, and furthermore, they harbor intratumoral heterogeneity.^{11,12} Recent studies suggest that metastases often originate from one subclone, not necessarily representing the highest GG.¹³ A recent systematic review on the genetic landscape of MRI-visible and invisible PCa concluded, that MRI-visible PCas are enriched with hallmarks of aggressive cancers, including growth, DNA damage and inflammation.¹⁴ Most studies are, however, conducted with non-case-matched cohorts, that is, low-grade MRI-invisible cancers are compared to higher grade MRI-visible cancers. This confounding by poorly constructed data sets complicates the interpretation of results. Since MRI-era cohorts are not mature enough to study survival directly, pre-MRI era cohorts are needed for survival analyses. Importantly, a post hoc analysis of the PROMIS trials was recently published where the authors concluded that GG alone is likely inadequate to account for lesion visibility on MRI. Further, they concluded that the major limitation of their study was the analysis on a per-patient level.

Specifically, men with concurrent visible and invisible lesion may have their invisible lesions overlooked due to an overall positive MRI finding generated by the visible lesion(s).¹⁵

Therefore, our aim was to study PCa histomic and transcriptomic characteristics associated with MRI visibility of PCa in a cohort with matched GG, pathological stage and prostate-specific antigen (PSA) on a per-lesion level. Transcriptomic signatures associated with tumor visibility were compared with expression of genes included in PCa risk stratification panels. Finally, we studied the association of the signatures to clinical outcomes of PCa, in an external case-control study with matched baseline characteristics.

2 | MATERIALS AND METHODS

2.1 | Patient summary

We studied a subset of PCa patients in the Finnprostate registry study combining Finnish national registry and hospital data. In an earlier study, we identified all men with a preoperative MRI undergoing robot-assisted laparoscopic RP ($n = 387$) at HUS Helsinki University Hospital (HUS), during 2014 to 2015.¹⁶ From these data, 30 patients were selected based on having an MRI-visible csPCa index lesion, defined as GG \geq 2 at final pathology and having the highest PI-RADS score. Of these, 10 had PI-RADS 3, 10 had PI-RADS 4 and 10 had PI-RADS 5 lesions. Another 15 patients were selected based on having at least one MRI-invisible csPCa lesion, defined as GG \geq 2 at final pathology. Further, the selected invisible lesion for the study was defined as the largest lesion in the RP specimen not recorded in the prostate MRI report, that is, "PI-RADS 0." Patients with an invisible lesion also had zero to three MRI-visible lesions. The cohort also included 19 benign controls, two of which were RP specimens without histology-confirmed PCa, and 17 trans-urethral resections from MRI-negative prostates due to benign prostatic hyperplasia in the years 2015 to 2018. Power calculations were not performed before initiation of the study.

Histological slides were re-evaluated by three expert uropathologists (Tuomas Mirtti, Stig Nordling and Kevin Sandeman) and representative areas were annotated for tissue sampling. Formalin-fixed

TABLE 1 Baseline characteristics of the study cohort.

| Variable | Visible ^a | Invisible | Benign | Visible vs invisible |
|--------------------------------------|----------------------|-------------|------------|----------------------|
| Sample type, n (%) | | | | |
| RP | 30 (100) | 15 (100) | 2 (11.1) | |
| TURP | 0 | 0 | 16 (88.9) | |
| Age (yr.) | | | | |
| Mean (SD) | 62.7 (7.1) | 62.7 (5.6) | 64.9 (8.4) | <i>P</i> = 1.0 |
| Tumor GG, n (%) | | | | <i>P</i> = .008 |
| 2 | 19 (63.3) | 15 (100) | | |
| 3 | 11 (36.7) | 0 | | |
| Maximum TMA punch GG, n (%) | | | | <i>P</i> = .70 |
| 1 | 4 (13.3) | 3 (20.0) | | |
| 2 | 13 (43.3) | 9 (60.0) | | |
| 3 | 9 (30.0) | 2 (13.3) | | |
| 4 | 3 (10.0) | 1 (6.7) | | |
| 5 | 1 (3.3) | 0 | | |
| pT stage, n (%) | | | | <i>P</i> = 1.0 |
| T2 | 22 (73.3) | 12 (80.0) | | |
| T3a | 7 (23.3) | 3 (20.0) | | |
| T3b | 1 (3.3) | 0 | | |
| Lesion location, n (%) ^b | | | | |
| Peripheral zone | 29 (96.7) | 15 (100) | | <i>P</i> = 1 |
| Transitional zone | 15 (50.0) | 3 (20.0) | | <i>P</i> = .063 |
| Anterior fibromuscular stroma | 12 (40.0) | 0 | | <i>P</i> = .004 |
| Central zone | 2 (6.7) | 3 (20.0) | | <i>P</i> = .31 |
| MRI tumor volume (ml) | | | | |
| Median (IQR) | 1.05 (1.3) | | | |
| Tumor diameter in PAD (mm) | | | | |
| Median (IQR) | 21.5 (11.0) | 16.0 (3.0) | | <i>P</i> = .027 |
| Pre-Surgery PSA (ng/ml) | | | | |
| Median (IQR) | 9.5 (5.3) | 8.1 (5.1) | 12.7 (7.3) | <i>P</i> = .60 |
| PSA-density (ng/ml/cm ³) | | | | |
| Median (IQR) | 0.22 (0.22) | 0.18 (0.25) | | <i>P</i> = .21 |
| ADC (μm ² /s) | | | | |
| Mean (SD) | 628 (187) | 919 (229) | | <i>P</i> < .001 |
| Histological variant, n (%) | | | | <i>P</i> = .15 |
| Mucinous | 8 (26.7) | 8 (53.3) | | |
| Foamy cell | 4 (13.3) | 0 | | |
| Cribriform | 0 | 1 (6.7) | | |
| Ductal | 1 (3.3) | 0 | | |
| Pseudohyperplastic | 1 (3.3) | 0 | | |
| Biochemical recurrence, n (%) | 5 (16.7) | 3 (20.0) | | <i>P</i> = 1.0 |

Abbreviations: ADC, apparent diffusion coefficient; GG, grade group; IQR, interquartile range; MRI, magnetic resonance imaging; PSA, prostate-specific antigen; pT stage, pathological TNM eighth edition cancer stage; RP, radical prostatectomy; TMA, tissue microarray; TURP, transurethral resection of the prostate.

^aProstate imaging-reporting data system (PI-RADS) 3 (n = 10), PI-RADS 4 (n = 10), PI-RADS 5 (n = 10).

^bSum of percentages may go over 100%, since lesions extended to multiple prostatic zones.

paraffin-embedded (FFPE) tissues were sampled to a tissue microarray (TMA) and for RNA extraction. In the end, one benign sample was excluded from analyzes due to outlier transcript counts. REMARK

diagram illustrating the flow of patients through the study can be found in Figure S1. The baseline characteristics of patients included in the analyses are described in Table 1.

2.2 | Case-control study for assessing clinically relevant outcomes

A previously described retrospective pre-MRI-era case-control cohort was used to assess metastasis-free survival (MFS) and cancer-specific survival (CSS) during an 11-year follow-up.¹⁷ The study included 160 patients with localized GG2-4 PCa at RP. Seventy-six of the men, representing cases, had metastatic progression during the follow-up and 49 of them died of PCa. Eighty-four men with baseline-matched disease, representing controls, had no metastatic or lethal progression during the follow-up. RNA had previously been extracted from FFPE blocks and was analyzed using the same methodology as for the current study cohort.

2.3 | Clinical MRI protocol and re-evaluation

The imaging was performed with a 3 T Philips Achieva device, and the protocol derived from PI-RADSv1, which was the guideline version at the time of the scans.⁴ The MRI included sagittal, axial and coronal T2 weighted (T2WI) and diffusion-weighted imaging (DWI) with apparent diffusion coefficient (ADC)-maps and dynamic contrast enhancement (DCE) sequence. The slice thickness was 3 mm for T2WI and DWI, and 4 mm for DCE. The T2WIs were obtained with turbo-spin-echo (TSE) sequence covering the whole prostate gland and seminal vesicles. The DWI utilized b-values 0, 100 and 800 for calculating ADC-maps, and b-value 2000 was scanned separately for tumor detection. The DCE imaging was performed with an intravenous gadolinium-based contrast agent (Dotarem, 0.2 ml/kg, 2 ml/s) with the temporal resolution of 8 s and a total acquisition time of 2.5 min to detect early enhancement. The DCE data were visually assessed and further analyzed using the scanner's software to produce signal-intensity curves of each detected lesion. The findings were reported in a structured manner presenting the number of lesions (max 4), location (sector map) and size (volume and max diameter) of each lesion, and local radiological staging (capsule contact length, extraprostatic extension, seminal vesicle invasion and lymph node metastasis).

The MRI scans were re-evaluated by a radiologist (JP) and ADC values were collected. The ADCs of the MRI-visible lesions were determined by measuring the lowest ADC of the apex, middle and base of the tumor. The ADCs of invisible lesions were measured from three subsequent slides based on their corresponding topographical locations in the histological RP slides. In the end, the ADCs measured from the middle slides were used in analyzes.

2.4 | Construction and analysis of the TMA

Two punches with a 1 mm diameter from representative tissues adjacent to those sampled for RNA analyses were transferred into TMA FFPE blocks. TMA sections of 3.5 μ m were stained with hematoxylin and eosin in a clinical laboratory (Huslab, Helsinki, Finland). The TMA slides were scanned using Panoramic 250 Flash III scanner

(3DHISTECH, Budapest, Hungary) and scans dearrayed. The de-arrayed cores were visually assessed by an uropathologist and a non-pathologist researcher (TM, TPL) for GG and histological variants. Then, QuPath v0.41 pixel classification was used for classifying and measuring epithelium, stroma and background using pixel classifier models.¹⁸ Eight models were trained to account for variance in staining intensity. All available features were used for classification. Annotations to train the models and the classification results were checked by a non-pathologist researcher (TPL). Finally, the segmentations were cleaned by annotating over the segmentation masks and measuring the number of incorrectly classified pixels. This number was then subtracted from the incorrect segmentation and added to the correct segmentation area. Luminal area was calculated from background by measuring the area of each TMA core and subtracting pixels in the background segmentation from outside of the core. Two TMA cores in the primary cohort, and three in the secondary cohort, were excluded due to being missed and containing no cancer.

2.5 | RNA extraction and transcriptomics analysis

RNA extraction and analysis were performed as published previously.¹⁷ Briefly, one to two 1 mm diameter cores were extracted from each annotated lesion and were deparaffinized, homogenized and proteinase K digested. RNA was extracted using QIASymphony (QIAGEN, Venlo, Netherlands) RNA kit and concentration assessed using RiboGreen kit (Invitrogen, Waltham, MA). RNA integrity (1.00-2.70, mean = 2.29, SD = 0.31) was measured with Agilent Bioanalyzer kit (Agilent Technologies, Santa Clara, CA). The transcript counts were measured with Nanostring nCounter (NanoString Technologies, Seattle, WA) platform at the DNA Sequencing and Genomics Laboratory, Institute of Biotechnology, University of Helsinki, Finland. Transcripts were detected by overnight incubation with Reporter and Capture CodeSet probes, specific to 794 cancer-related genes, six housekeeping genes, eight spike-in negative and six positive controls.¹⁷ The CodeSet contained the genes included in the commercially available PCa risk stratification panels including Decipher (Veracyte, San Diego, CA), Oncotype DX (Exact Sciences, Madison, WI), Prolaris (Myriad Genetics, Salt Lake City, UT), and the pan-cancer mutational panel MSK-IMPACT (Memorial Sloan Kettering Cancer Center, New York, NY).

2.6 | Statistical analysis

Quality control for transcript analyses were performed in nSolver Analysis Software (NanoString Technologies), v. 4.0.70. Other analyses were performed in R, v.4.2.1 (R Development Core Team, Vienna, Austria). Continuous clinical variables were analyzed with Student's two-tailed *t*-test if they were normally distributed in the Shapiro-Wilk test. Mann-Whitney *U*-test was used for non-normal continuous and ordinal data. Dichotomous variables were studied with Fisher's test. Spearman correlation was analyzed between tissue

areas and ADC. Mean tissue component areas were calculated from the two TMA cores of each patient before using Mann-Whitney *U*-test.

Positive control linearity and coefficients of variance for housekeeping genes were calculated. Limit of detection (LOD) was defined as mean of negative controls and genes with mean expression under LOD were excluded. Upper-quartile normalization was performed, and factors of unwanted variation estimated using housekeeping genes. Counts were then variance stabilizing transformed.

Hierarchical clustering of samples was performed using the complete-linkage method and Kendall correlation distance. The clustering performance was measured by comparing the clusters to study group labels using adjusted Rand index (ARI) with the tree split to two and three clusters.

Counts of visible and benign samples were separately compared to invisible samples in differential expression analysis. The differentially expressed genes (DEGs) were defined as Benjamini-Hochberg adjusted *P* (*P*.adj) < .05 in Wald test and $|\log_2(\text{fold change})| > 0.585$. Reactome pathway analysis was performed for up- and downregulated DEGs. The pathways were filtered using *P*.adj < .05.

The associations of TMA core-derived tissue areas, and DEGs, with survival were separately analyzed in the case-control study with Kaplan-Meier. Patients were stratified for survival analysis based on higher or lower than median tissue area or DEG expression, respectively. Event-free survival was defined as days between RP and the detection of metastases or PCa-specific death (PCSD), respectively, or as the time between RP and the last recorded patient contact. *P* values were Benjamini-Hochberg adjusted.

Random forests (RFs) were trained to classify MRI visibility using DEGs, and the transcripts included in the commercial risk stratification panels. The data was split into training (67%) and validation sets (33%). Ten times repeated 3-fold stratified cross-validation was used during training and hyperparameter tuning and AUC was used to measure classification performance. Hyperparameters *m*try (1-1.5 × sqrt [*n*]) and minimum node size (1-5) were tuned. Synthetic minority over-sampling technique was used inside folds of training data. RFs were similarly trained to classify metastasis and PCSD in the case-control study with six times repeated 5-fold stratified cross-validation. DeLong method was used to calculate confidence intervals for AUCs. Survival analysis was performed by separately comparing the true survival of those with RF predicted metastatic and lethal disease to those with no predicted endpoint.

3 | RESULTS

3.1 | Clinical characteristics do not explain differences in MRI visibility

We first evaluated whether MRI visibility could be explained by clinicopathological variables (Table 1). As expected, the visible lesions had higher GG and lower ADC values (*P* < .01 for both) than the invisible lesions. The differences in tumor pathological stage, preoperative PSA

or PSA-density (PSA-D) were statistically insignificant. Moreover, the invisible lesions were missed on radiologist re-evaluation, whereas all PI-RADS 3-5 lesions were visible. The invisible lesions were smaller than visible ones (*P* = .027). All but one (*n* = 29) of the visible lesions and all (*n* = 15) invisible lesions were at least partially located in the peripheral zone.

3.2 | MRI-invisible lesions harbor histological components closer to benign tissue than cancer

Representative examples of TMA histological sections from each study group are shown in Figure 1A and one section overlain with a segmentation mask used to calculate tissue areas in Figure 1B. We found no statistically significant differences in the frequency of histological variants between study groups. However, this might be due to lack of statistical power, since mucinous histology was twice as frequent in the MRI-invisible lesions compared to the visible group (Table 1). There were no statistically significant differences in the area occupied by epithelium or stroma between the cancer groups (*P* > .05 for both; Figure 1C, D), although the MRI-visible PCas seemed to have generally higher epithelial area, compared to invisible lesions. However, luminal area was lower in MRI-visible group compared to invisible PCa or benign prostates (*P* < .01), while no differences were found between invisible and benign groups (Figure 1E). Luminal area was also found to be lower in the aggressively behaving cases compared to indolent controls (Figure 1C-E) and low luminal area was associated with short MFS and CSS (*P* < .05 for both; Figure S2). We found no correlation between the tissue compartments and ADC (Figure S3).

3.3 | Differentially expressed genes based on lesion MRI visibility associate with prognosis

As expected, hierarchical clustering of all analyzed transcript counts showed separation of benign samples from cancerous ones (ARI = 0.87; Figure 1F), when the tree was split into two clusters. Visible and invisible lesions also formed subclusters, although they did not separate as clearly from each other as from benign, leading to lower ARI (0.34) when the tree was split into three clusters (Figure 1F).

In a differential gene expression analysis between the MRI-visible and invisible lesions, we identified 67 DEGs (Figure 1G). Of these, 24 were upregulated, and one downregulated, in visible compared to invisible PCa and had a linear direction of change in expression from benign to invisible and invisible to visible. We call these “linear pattern”, emphasized by yellow color in Figure 2. Furthermore, eight DEGs were similarly expressed (ie, $|\log_2(\text{fold change})| \leq 0.585/2$) between invisible and benign but upregulated in visible PCa lesions. This pattern of gene expression we call “sigmoid pattern”, emphasized by purple color in Figure 2. The remaining 34 DEGs we call a group with “non-monotonical” gene expression pattern across the study

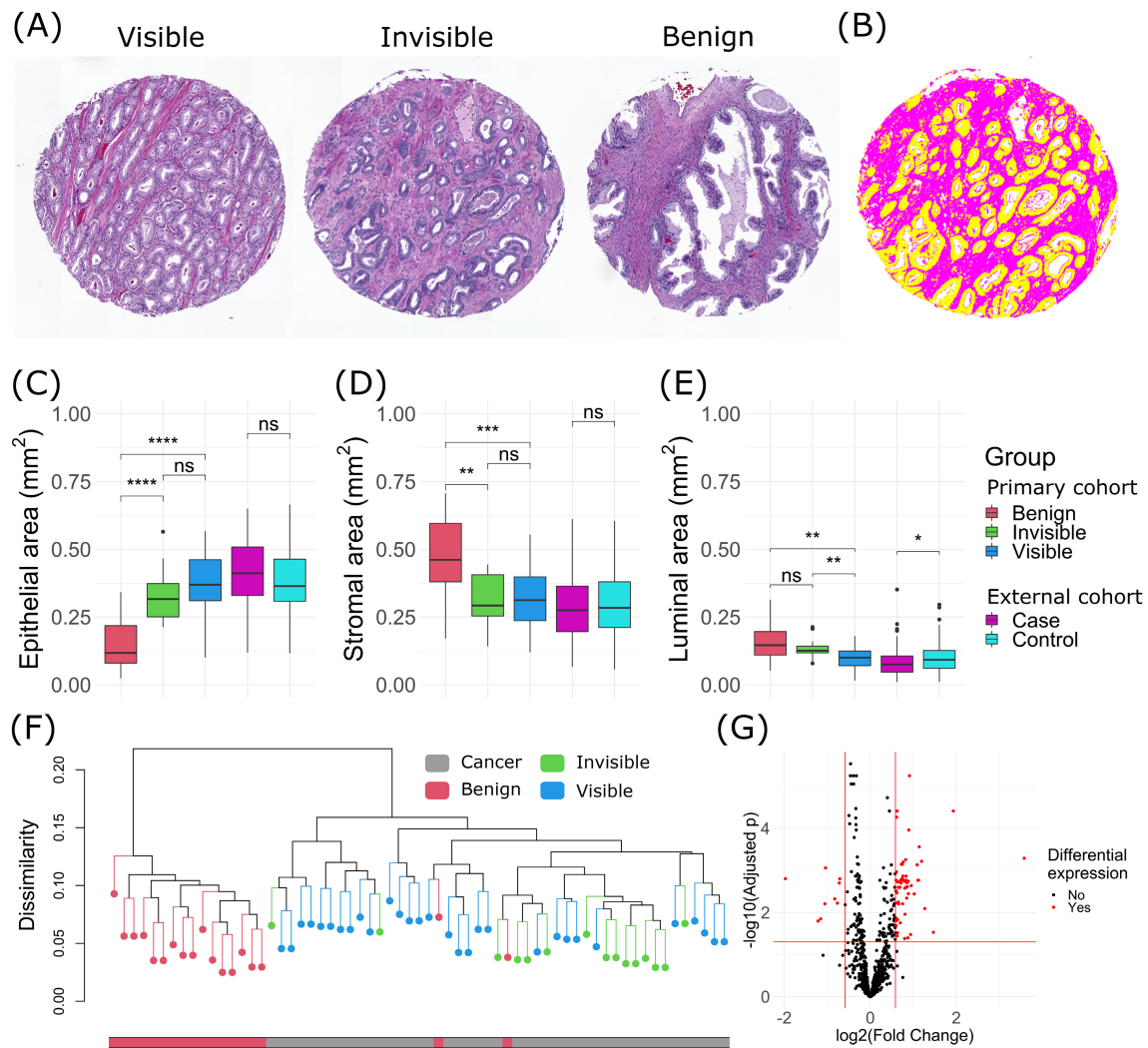


FIGURE 1 Quantitative histopathology and exploratory transcript analysis. (A) Representative tissue microarray cores of each group. (B) Example of segmentation into epithelium (yellow), stroma (purple) and background (white) based on a pixel classifier model trained in QuPath. (C–E) Magnetic resonance imaging (MRI)-visible lesions have lower luminal area fraction compared to invisible lesions based on QuPath segmentations. Similarly, aggressive cases have lower luminal area compared to indolent controls in the external material. Center-line represents median, hinges the interquartile range (IQR), and whiskers $1.5 \times \text{IQR}$ from hinge. Mann-Whitney *U*-test *P* values: ns, non-significant ($P > .05$). $*P < .05$; $**P < .01$; $***P < .001$; $****P < .0001$. (F) Hierarchical clustering of all studied samples based on read counts of all analyzed transcripts. Most of the benign samples expectedly form a single cluster, while the MRI-visible and MRI-invisible samples form smaller subclusters. (G) Volcano plot showing the distribution of differentially expressed genes between MRI-visible and invisible prostate cancers. Horizontal red line represents Benjamini-Hochberg adjusted Wald-test *P* value threshold of 0.05 and vertical lines \log_2 fold changes of -0.585 and 0.585 .

groups, emphasized by the gray color in Figure 2. In non-monotonical group, gene expression in the invisible lesions was downregulated or upregulated compared to both benign and visible PCa. In the non-monotonical pattern group, 26 DEGs were upregulated, and eight downregulated, in visible compared to invisible. The three DEG groups; linear, sigmoid and non-monotonical pattern, were considered in further analyzes, in addition all DEGs combined.

We studied the association of DEG expression levels and clinically relevant outcomes by analyzing MFS and CSS in the external case-control cohort (Table 2, Figure S4). Of the linear pattern DEGs, two were significantly associated with MFS, and three with CSS ($P_{\text{adj}} < .05$ for all). One sigmoid pattern DEG was associated with

CSS ($P_{\text{adj}} = .013$). Finally, four non-monotonical pattern DEGs were associated with CSS ($P_{\text{adj}} < .05$ for all). The expression pattern of MRI-visible PCa was associated with poor prognosis in six of the eight DEGs.

3.4 | Pathway analysis reveals mechanisms associated with MRI visibility

We performed Reactome pathway over-representation analysis, to identify biological pathways associated with MRI visibility (Figure 3). The linear pattern DEGs, upregulated in visible samples,

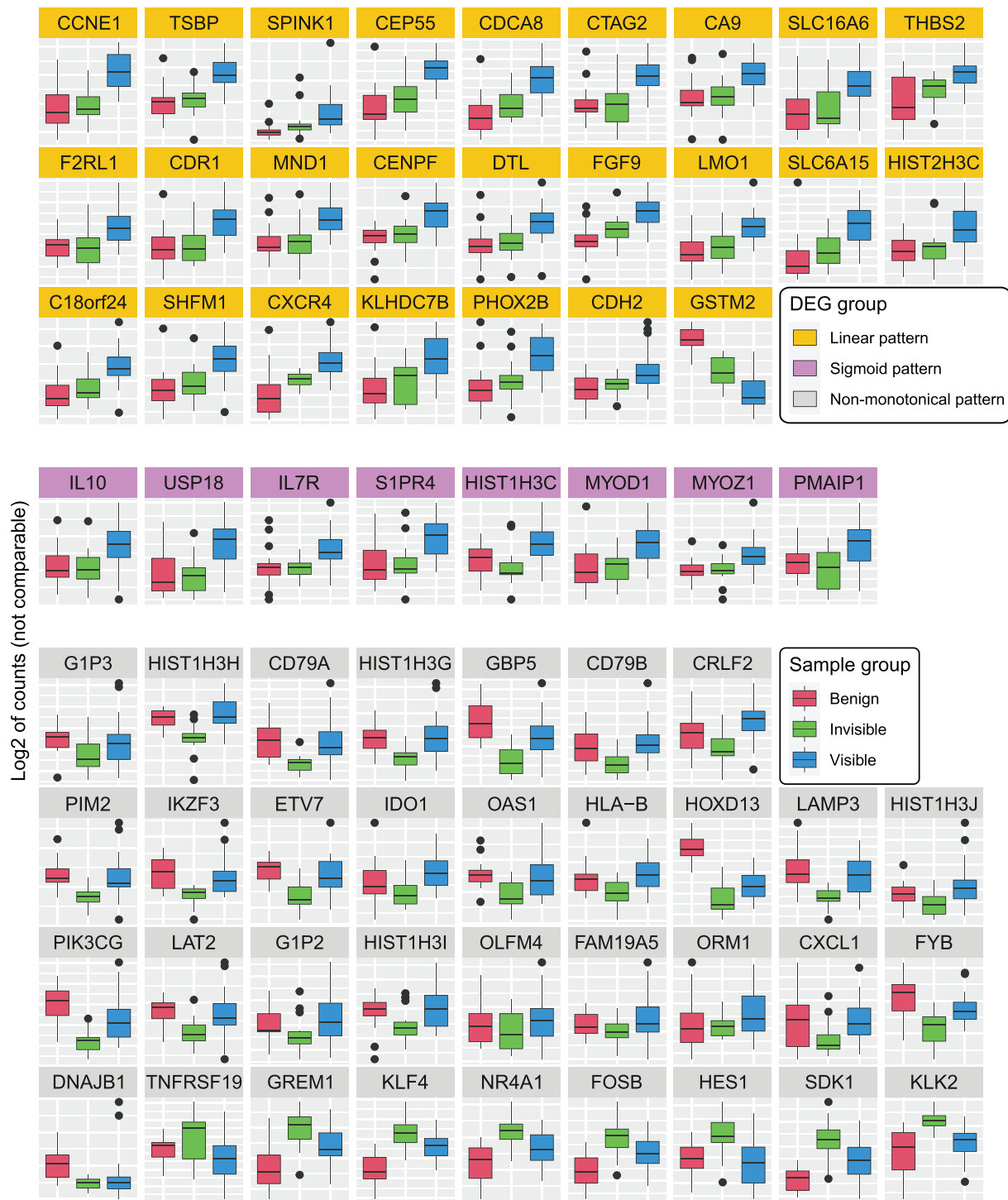


FIGURE 2 Panel of boxplots depicting the differentially expressed genes (DEGs) in MRI-visible prostate cancer (PCa) compared to invisible lesions. DEGs were categorized into three groups based on the expression change from benign to MRI-invisible and to MRI-visible. Twenty-five DEGs showed a linearly increasing, or decreasing, expression pattern from benign to invisible and from invisible to visible group. Eight DEGs only showed a change in expression between magnetic resonance imaging (MRI)-visible and invisible lesions, but no change between MRI-invisible PCa and benign samples. 34 DEGs showed a non-monotone expression pattern, that is, the direction of differential expression was the same between MRI-invisible and visible PCAs, as well as between invisible PCAs and benign prostates. Center-line represents median, hinges the interquartile range (IQR), and whiskers $1.5 \times$ IQR from hinge.

were over-represented in 13 pathways. Similarly, upregulated sigmoid pattern DEGs were over-represented in two pathways. The non-monotonical pattern DEGs upregulated in visible lesions were

over-represented in 68 pathways. No pathways were identified based on downregulated DEGs in visible compared to invisible PCa. The pathways identified with the linear pattern DEGs were associated

TABLE 2 Differentially expressed genes between MRI-visible and invisible prostate cancer lesions are associated with survival.

| DEG group | DEG | Survival (P_{adj}) | | Prognostic impact of upregulation | Expression in visible vs invisible |
|--------------|----------|------------------------|--------------|-----------------------------------|------------------------------------|
| | | Metastasis-free | PCa-specific | | |
| Linear | HIST2H3C | .008 | .01 | Negative | Upregulated |
| | THBS2 | .12 | .04 | Negative | Upregulated |
| | FGF9 | .03 | .01 | Positive | Upregulated |
| Sigmoid | HIST1H3C | .05 | .01 | Negative | Upregulated |
| Non-monotone | HIST1H3H | .06 | .01 | Negative | Upregulated |
| | CRLF2 | .47 | .04 | Positive | Upregulated |
| | FOSB | .17 | .03 | Positive | Downregulated |
| | NR4A1 | .14 | .01 | Positive | Downregulated |

Note: Only those, with statistically significant association with survival, after Benjamini-Hochberg adjustment for multiple hypothesis testing are shown. Kaplan-Meier survival curves are shown in Figure S3. Significant P values ($P_{adj} < .05$) are bolded. Abbreviations: DEG, differentially expressed gene; P_{adj} , Benjamini-Hochberg adjusted P value; PCa, prostate cancer.

with cell-cycle and proliferation. The sigmoid pattern DEGs were over-represented in inflammatory interleukin signaling related pathways and non-monotonical pattern DEGs in regulation of gene expression.

3.5 | Gene expression panels based on DEGs are associated with MRI visibility

Next, we established a benchmark of MRI visibility classification performance, by training RFs with all DEGs in visible vs invisible comparison ($n = 67$) as well as linear, sigmoid and non-monotonical pattern DEGs. In addition to DEGs, the clinical parameters GG, pathological stage and PSA were included as predictors. All models based on DEGs expectedly showed excellent classification performance (area under the curve [AUC] = 0.90-1) (Figure 4A), since the DEGs were chosen based on differences in expression between MRI-visible and invisible csPCa lesions. The clinical parameters improved prediction performance negligibly, and showed poor prediction performance alone (AUC = 0.60). ROC curves of panels without clinical parameters can be found in Figure S5A-C.

3.6 | Expression levels of genes in commercial prognostic panels are associated with MRI visibility

We sought to determine whether the expression levels of genes included in the commercial prognostic panels associate with MRI visibility of PCa. We visualized transcript levels of genes included in Decipher, MSK-IMPACT, Oncotype DX and Prolaris with heatmaps (Figure S6A-D). We also studied their ability to predict MRI visibility with RFs (Figure 4B). MSK-IMPACT showed the highest prediction performance (AUC = 0.94, CI = 0.83-1), while Decipher (AUC = 0.86, CI = 0.65-1) and Oncotype DX (AUC = 0.92, CI = 0.78-1) also showed good performance. Prolaris performed worse in this analysis (AUC = 0.64, CI = 0.2-1). Interestingly, three of the four panels

showed high prediction performance, despite not sharing any common genes (Figure S7).

3.7 | Expression levels of MRI visibility-associated DEGs predict prognosis

Next, we studied whether our visibility-associated signatures were also associated with prognosis in a separate baseline-matched case-control cohort. RFs were trained to predict metastatic PCa and PCSD (Figures 4C, D and S5B-C). Linear pattern DEGs combined with clinical variables showed the highest metastasis prediction performance (AUC = 0.73, CI = 0.59-0.87). In PCSD prediction, linear (AUC = 0.65, CI = 0.47-0.83) and non-monotonical pattern DEGs (AUC = 0.66, CI = 0.49-0.83) combined with clinical variables showed similar performance. Again, the clinical parameters alone, were not predictive of either metastatic disease or PCSD (AUC = 0.54 for both). However, they slightly, but consistently improved metastasis, but not PCSD prediction performance.

Finally, we performed Kaplan-Meier analysis to validate RF classification results. Patients were stratified for survival analysis based on RF classification, and their ground truth MFS and CSS compared. Linear pattern DEGs combined with clinical parameters showed significant difference in survival between patients predicted to have metastatic and non-metastatic disease ($P = .024$; Figure S8A). Furthermore, predictions of non-monotonical pattern DEGs alone, or combined with clinical parameters, associated with CSS ($P = .026$ and $P = .047$, respectively; Figure S8B-C).

4 | DISCUSSION

MRI is increasingly applied to PCa diagnostics as a triage test and to target biopsies. However, there is an ongoing debate on whether systematic biopsies should be used in conjunction with TBx, since 9% to 24% of csPCa lesions are invisible in MRI.^{9,10} This also reflects the

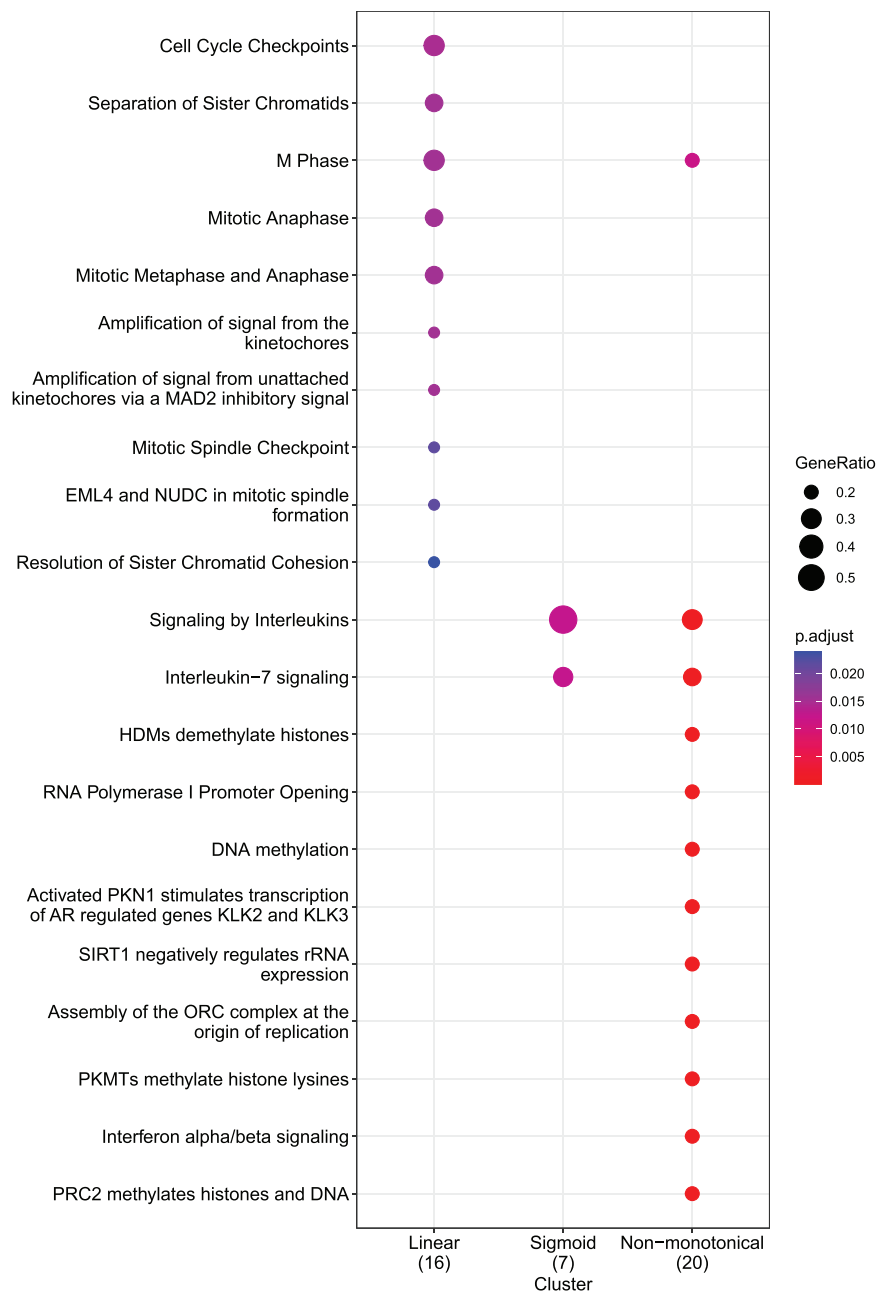


FIGURE 3 Most significant upregulated pathways in magnetic resonance imaging-visible prostate cancers. The pathway analysis was separately performed for the differentially expressed gene (DEG) groups. The linear pattern DEGs were over-represented in proliferation-related pathways. Sigmoid pattern DEGs were enriched in inflammatory interleukin-7 signaling and non-monotone pattern DEGs in pathways associated with the regulation of transcription. *P* values are calculated using the binomial test.

uncertainty around focal therapy. However, little is known about the genetic characteristics and clinical significance of these MRI-invisible lesions. While clinical follow-up of the men with MRI-invisible lesions is the ultimate means of resolving this knowledge gap, no cohorts with sufficient follow-up time exist today. In our data, only a fifth of the patients with follow-up data experienced BCR, the first surrogate of poor prognosis. Therefore, we set out to study the MRI-invisible lesions on histologic and transcriptomic levels and linked our findings to a pre-MRI-era cohort to study survival. Our findings indicate that low luminal area is one of the histological determinants of PCA MRI visibility and is also associated with poor MFS and CSS. Further, MRI-visible lesions harbor transcriptomic features, which are also associated with shorter MFS and CSS, than invisible lesions. Taken together, our findings support TBx-only strategy for PCA diagnostics.

We first re-evaluated the MRI sequences and confirmed that the studied MRI-invisible lesions were truly invisible, and not missed due to poor radiologist performance. This per-lesion analysis is important as currently the invisible lesions may be overlooked in overall MRI-positive patients, in a per-patient analysis. We next analyzed the association of clinical variables, histology and MRI variables with the visibility status. As expected, lesion GG was associated with MRI visibility, similar to, for example, PROMIS trial.¹⁵ However, all lesions were GG2-3, and it has been shown that the proportion of Gleason grade pattern 4 in GG2-3 PCs is not the key determinant of MRI visibility.¹⁹⁻²² In-line with our results, a recent study showed that patients with MRI-visible GG1-2 lesions, had shorter treatment-free survival and higher risk of Gleason upgrading than those with invisible lesions.²³ MRI-invisible lesions were, on

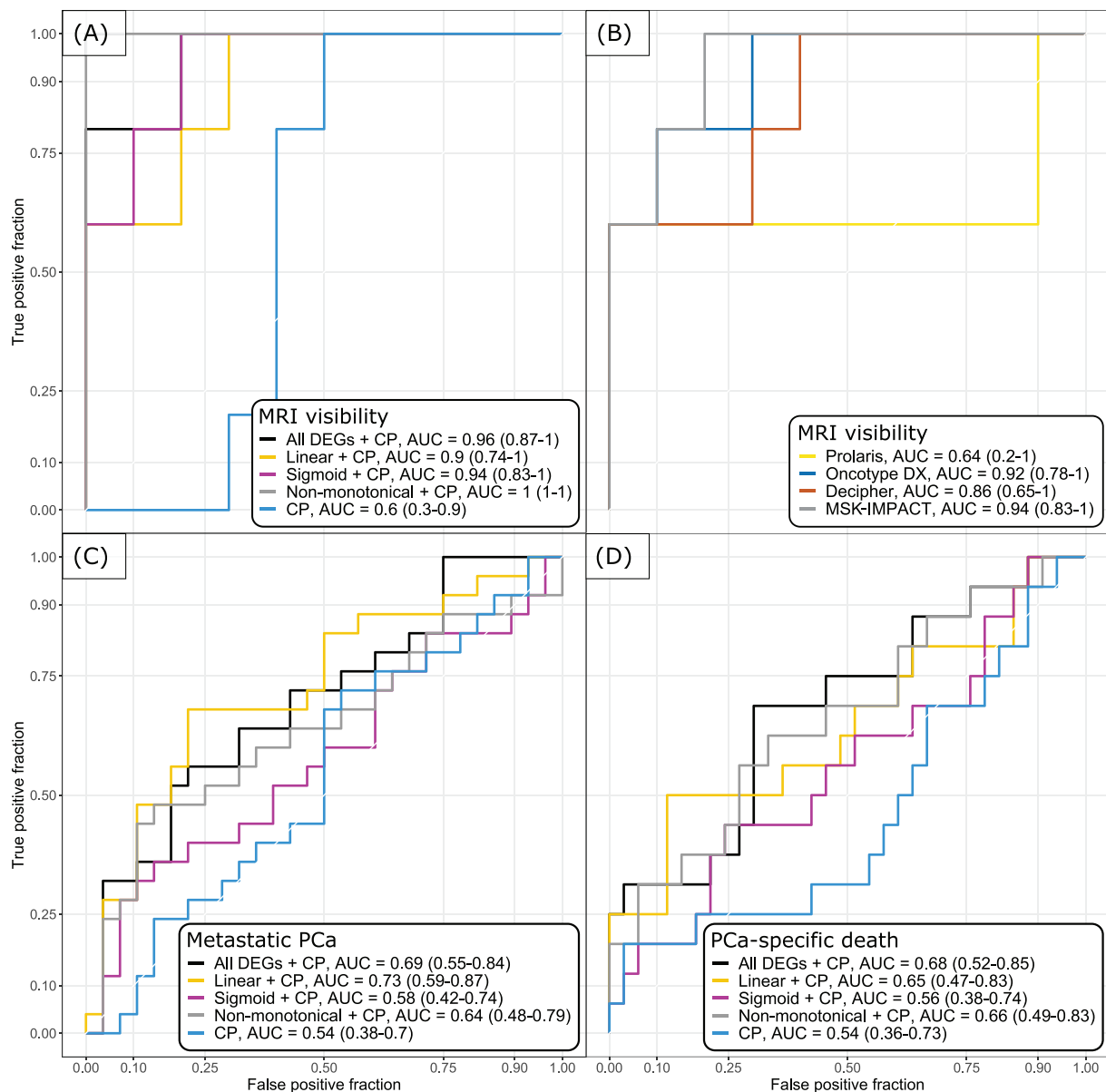


FIGURE 4 Receiver operating characteristic (ROC) curves for predicting MRI-visibility and post-operative survival based on random forest analysis. (A) The differentially expressed gene (DEG) groups combined with clinical parameters (grade group, pathological stage and prostate-specific antigen) outperformed the clinical parameters alone in classification of prostate cancer (PCa) as MRI-visible and invisible in the validation set. (B) The publicly available genes included in the commercial panels Decipher, Oncotype DX, as well as the pan-cancer mutational panel MSK-IMPACT outperformed Prolaris and the clinical parameters in MRI visibility classification. (C) All visibility-associated DEGs, linear and non-monotone pattern DEGs combined with clinical parameters outperformed the clinical parameters alone in prediction of metastatic disease in an external case-control study with 11 years of follow-up. (D) Similar results were obtained in prediction of PCa-specific death, using DEGs and clinical parameters as independent variables. DeLong confidence intervals are in parentheses. CP, clinical parameters (grade group, pathological stage and prostate-specific antigen).

average, smaller than MRI-visible lesions. However, all invisible lesions were at least 14 mm in diameter (median 16 mm), which considering previous research should be large enough to be detected in MRI.^{5,19,24} In concordance with our data is the post-hoc analysis of the PROMIS trial where most of the MRI visible- and invisible lesions were GG2 suggesting that other factors such as tissue composition play a role in MRI visibility.¹⁵ Interestingly, and contrary to our findings, PSA-D has been shown to be associated

with increased risk of MRI-invisible PCa in biopsies, in patients with additional MRI-positive lesions.²⁵

We next hypothesized, that the tissue compartment volumes, that is, the epithelial, stromal and luminal content in the MRI-invisible lesions was closer to benign, than that of visible lesions. We observed, that the amount of luminal space was lower and epithelial area was higher in MRI-visible PCa compared to invisible PCa, although the latter was not statistically significant different. This corroborates the

existing evidence of correlation between tissue compartment volumes and Gleason grades and ADC values and supports the hypothesis that MRI-invisible lesions are more indolent than MRI-visible lesions.²⁶⁻²⁸

Of the PCa histological variants, the cribriform pattern and ductal PCa, have previously been associated with low conspicuity on prostate MRI,^{19,29} although contradicting evidence also exists.^{20,30} Intraductal pattern has been linked with increased MRI visibility,^{30,31} but it also correlates with higher GG. In our cohort, there was only one lesion presenting with a cribriform pattern in the TMA, which indeed, belonged to the MRI-invisible group. On the other hand, the visible group had a lesion with ductal pattern. The major histological variant in our cohort was mucinous adenocarcinoma, which was twice as frequent in invisible lesions (53%) compared to visible ones.

Next, we sought to evaluate differences in gene expression of MRI-visible and invisible lesions and benign prostate as a surrogate to study the clinical significance of MRI-invisible lesions. Li et al have previously identified a set of four genes linked to MRI visibility, progression-free survival and metastatic disease.³² Of these four genes, *CENPF*, and *ALDH2* were included in our gene panel. We confirmed, that *CENPF* was upregulated in MRI-visible PCa, but it did not remain significantly associated with survival after multiple hypothesis testing adjustment. On the contrary, we failed to confirm the association of *ALDH2* gene expression with PCa visibility on MRI. Although the identified genes associated with tumor visibility differ between the studies, the overall results are comparable, with the main finding being, that MRI-invisible lesions harbor a less aggressive transcriptomic profile. The limitation of the study by Li et al is, that the invisible lesions were GG1-2, whereas visible lesions were GG2-5 PCa. Therefore, the gene expression data may reflect more the transcript level differences between low and high grade PCa, not MRI visibility.

The studied NanoString CodeSet included transcripts previously identified to be genomic hallmarks of aggressive PCa, including *PTEN* (data not shown). We did not find significant differences in expression levels of *PTEN* between MRI-visible and invisible group (data not shown). *PTEN* loss is associated with lower ADC values in MRI, when GG is not accounted for.³³ In the study by Switlyk et al, GG was negatively correlated with ADC, as was *PTEN* expression, which might reflect mainly differences in GG.³³ In another study, *PTEN* expression was not associated with ADC, but with forward volume transfer constant, another quantitative MRI parameter.³⁴ Again, GG was similarly correlated with *PTEN* expression, masking the role of MRI visibility.

Contrary to *PTEN*, to our knowledge, there is no evidence on the association of MRI visibility and other widely studied PCa tumor suppressor genes or oncogenes. In our data (not shown), *ERG* was highly expressed in both cancer groups. *Androgen receptor (AR)*, which is downregulated in *ERG*-positive PCa, was downregulated in visible PCa compared to benign, but was not associated with MRI-visibility. Loss of *AR* is linked to *MYC* amplification,³⁵ which we, again, found between benign and PCa, whereas no differences were observed between visible and invisible lesions. *SPOP*, which is downregulated or mutated in many cancers including PCa,³⁶ was statistically significantly downregulated in MRI-visible compared to invisible PCa ($P_{\text{adj}} = .003$), although it did not fulfill our $\log_2(\text{fold change})$ criteria

for a DEG. Interestingly, both cancer groups overexpressed *SPOP* compared to benign. In vitro, PCa cells have been shown to escape *SPOP*-mediated inhibition of proliferation and migration by overexpression of *CCNE1*.³⁷ Here, *CCNE1* was identified as a DEG and MRI-visible lesions had significantly higher *CCNE1* expression compared to invisible lesions, again suggesting less aggressive phenotype for MRI-invisible lesions. No differences in the expression levels of *IDH1* or *TP53* were found between study groups. We speculate, that these results are partially explained by our careful matching of the cancer groups and are more common in advanced PCa. Additionally, all studied PCas were localized and hormone-naïve at the time of RP, and none of the patients have developed castration-resistance or imaging-confirmed metastatic disease during the follow-up of 7.5 years. Thus, the analyzed RP tissues represent clinically early PCa.

Next, we set out to review the literature for our 67 DEGs that associate with lesion visibility in prostate MRI. A non-systematic literature review can be found in the Data S1. Several of the identified genes have previously been associated with aggressive PCa or other cancers. The upregulation or downregulation of these genes has been linked to, for example, high Gleason score, advanced stage, castration-resistance, neuroendocrine differentiation, short BCR-free, metastasis-free and disease-specific or overall survival in clinical cohorts. In *in vitro* cell models and mouse xenografts, several of the DEGs were associated with proliferation, epithelial-mesenchymal transformation, invasion and migration, metastasis, modification of antitumor immune response, angiogenesis and stromal reactivity. The expression pattern of majority of DEGs in our MRI-visible lesions was associated with poor outcomes or aggressive behavior in cell models in literature. The literature review was also in-line with our Reactome pathway analysis results, where the MRI-visible lesions had upregulated pathways related to proliferation, inflammatory cytokine signaling and regulation of transcription.

Finally, we hypothesized that transcriptomic risk stratification panels could classify MRI-visibility of prostate lesions, if visible and invisible lesions had different prognostic significance. Therefore, we analyzed the ability of publicly available transcripts included in the commercial risk stratification panels to classify MRI visibility as well as the prognostic value of DEGs. Decipher, Oncotype DX and MSK-IMPACT showed comparable MRI visibility classification performance with our DEGs and outperformed clinical parameters. Again, these data support the different prognostic significance of prostate lesions based on the visibility on MRI. Furthermore, DEGs chosen based on differences in MRI visibility are associated with patient important endpoints, that is, metastasis and PCa death, in an external cohort.

The major limitation of our study is comparison of MRI-invisible and visible lesions, instead of comparing completely MRI-negative patients to those with MRI-visible lesions. Because of this limitation, in addition to lack of follow-up during the MRI-era, we had to extract potentially prognostic features from the MRI-cohort, and use a pre-MRI-era cohort to test their impact on prognosis. Further, our benign controls have the limitation of being TURPs instead of RPs like the other study groups. TURPs are derived mostly from the central part of

the prostate, instead of the peripheral zone, which gives rise to most PCa. Further, TURPs do not contain conclusive evidence of lack of PCa outside of the resected tissue. To this end, we have confirmed, that none of the patients in the “benign” group, have been diagnosed with PCa to this day.

Since we only analyzed a panel of 800 transcripts instead of the entire transcriptome, it is likely, that there are additional genes contributing to MRI visibility, not captured by our analysis. Additionally, we studied a small number of patients, which reduces the statistical power of our results. Another limitation of our study, which is common to all the studies in the field, is the effect of heterogeneity of PCa. We showed that GG can vary significantly, when only a small section, such as a 1 mm TMA punch is considered, even if lesion level GG is matched. The TMA punches are representative of the amount of tissue used for bulk RNA analyses. Thus, intratumoral heterogeneity can generate sampling error even in a well-baseline-matched settings. To account for intratumoral, and intertumoral heterogeneity inherent to PCa, future spatial transcriptomics studies will be of significant interest.³⁸ Further, more advanced histomic image analysis techniques, such as unsupervised deep learning should be deployed in exploring differences between visible and invisible lesions in future studies to avoid possible bias in handcrafted selection of image features.

Although we have shown, that MRI-invisible lesions harbor less aggressive characteristics than visible lesions, they might still be drivers of prognosis in MRI-negative men. Promising techniques have been proposed to increase MRI-based detection of csPCa, including luminal water imaging (LWI), restriction spectrum imaging (RSI) and vascular, extracellular and restricted diffusion for cytometry in tumors (VERDICT).³⁹⁻⁴¹ However, the only way to capture true clinical significance of MRI-invisible lesions is to systematically follow men with a completely negative MRI. Arbitrary GG criteria for clinical significance, for example, the ones used in the PROMIS trial, or transcriptomic signatures, such as ours, are merely a surrogate. To this end, our ongoing randomized population based PCa screening trial (ProScreen), which is powered for PCa mortality, will provide the clinical follow up needed. In ProScreen trial, 120 000 men are randomized to screening and control groups. Screening is based on PSA, kallikrein panel and prostate MRI. Men with a negative MRI will not be biopsied, and are instead systematically followed with repeated screening rounds.⁴²

Taken together, our results suggest that PCa tumor visibility on MRI is a net result of many genes, which are associated with increased proliferation, inflammation and regulation of transcription. This likely translates to different tissue compartment volumes between MRI-invisible and MRI-visible lesions. Our data, combined with the extensive literature review, also suggests that MRI-visible PCa lesions harbor a transcript signature associated with more aggressive phenotype compared to invisible ones. Our results suggest, that in patients with a positive MRI, the additional MRI-negative PCa lesions may not be the drivers of poor prognosis. Thus, sampling MRI-visible lesions with TBx should be sufficient for accurate risk stratification in localized PCa.

AUTHOR CONTRIBUTIONS

The work reported in the article has been performed by the authors, unless clearly specified in the text. Timo-Pekka K. Lehto: Data curation, formal analysis, investigation, methodology, visualization, writing—original draft, writing—review & editing. Juho Pylväläinen: Data curation, formal analysis, writing—review & editing. Kevin Sandeman: Data curation, writing—review & editing. Anu Kenttämies: Writing—review & editing. Stig Nordling: Data curation, writing—review & editing. Ian G. Mills: Resources, Writing—review & editing. Jing Tang: Methodology, writing—review & editing. Tuomas Mirtti: Funding acquisition, supervision, writing—review & editing. Antti Rannikko: Conceptualization, funding acquisition, project administration, resources, supervision, writing—review & editing.

ACKNOWLEDGEMENTS

The authors thank Sanna Iikkanen and Jenni Niinimäki for core punching and sample preparation for RNA extraction. We thank Susanna Lauttia and Harri Sihto for helping with RNA extraction and sample preparation for transcript analysis. We thank Lars Paulin for the help in Nanostring nCounter analysis. We thank Adrian Malén for helping with data collection and Annikki Löfhjelm for excellent technical assistance. We thank Tolou Shadbahr for guidance in the theory of random forest algorithms.

FUNDING INFORMATION

Antti Rannikko reports grants from State Research Funding (VTR) of HUS Helsinki University Hospital, Finnish Cancer Organizations and Jane and Aatos Erkko Foundation. Tuomas Mirtti reports grants from State Research Funding (VTR) of HUS Helsinki University Hospital, Cancer Foundation Finland and Academy of Finland. Jing Tang reports grants from Academy of Finland.

CONFLICT OF INTEREST STATEMENT

The authors declare no conflicts of interest.

DATA AVAILABILITY STATEMENT

The data that support the findings of this study are available from the corresponding author upon reasonable request.

ETHICS STATEMENT

This study was approved by the institutional ethical review board of HUS (HUS/1439/2018) and the National Supervisory Agency for Health and Welfare (Dnro V/38176/2018). The research was conducted in compliance with the good research practice of the World Medical Association Declaration of Helsinki. The data was handled according to national laws and EU regulations. Since the study in question is a registry study, no explicit consent was required according to national legislation.

ORCID

Timo-Pekka K. Lehto  <https://orcid.org/0000-0003-3262-2333>

Juho Pylväläinen  <https://orcid.org/0000-0003-3192-3759>

Kevin Sandeman  <https://orcid.org/0000-0002-5019-6254>

Anu Kenttämies  <https://orcid.org/0000-0002-3937-5307>
 Stig Nordling  <https://orcid.org/0000-0001-5555-6645>
 Jing Tang  <https://orcid.org/0000-0001-7480-7710>
 Tuomas Mirtti  <https://orcid.org/0000-0003-0455-9891>
 Antti Rannikko  <https://orcid.org/0000-0002-4261-3484>

REFERENCES

- Sung H, Ferlay J, Siegel RL, et al. Global cancer statistics 2020: GLOBOCAN estimates of incidence and mortality worldwide for 36 cancers in 185 countries. *CA Cancer J Clin.* 2021;71:209-249.
- Mottet N, van den Bergh RCN, Briers E, et al. EAU-EANM-ESTRO-ESUR-SIOG guidelines on prostate Cancer-2020 update. Part 1: screening, diagnosis, and local treatment with curative intent. *Eur Urol.* 2021;79:243-262.
- Epstein JI, Egevad L, Amin MB, et al. The 2014 International Society of Urological Pathology (ISUP) consensus conference on gleason grading of prostatic carcinoma: definition of grading patterns and proposal for a new Grading system. *Am J Surg Pathol.* 2016;40:244-252.
- Barentsz JO, Richenberg J, Clements R, et al. ESUR prostate MR guidelines 2012. *Eur Radiol.* 2012;22:746-757.
- Weinreb JC, Barentsz JO, Choyke PL, et al. PI-RADS prostate imaging: reporting and data system: 2015, version 2. *Eur Urol.* 2016;69:16-40.
- Turkbey B, Rosenkrantz AB, Haider MA, et al. Prostate imaging reporting and data system version 2.1: 2019 update of prostate imaging reporting and data system version 2. *Eur Urol.* 2019;76:340-351.
- Venderink W, van Luijckelaar A, Bomers JGR, et al. Results of targeted biopsy in men with magnetic resonance imaging lesions classified equivocal, likely or highly likely to be clinically significant prostate cancer. *Eur Urol.* 2018;73:353-360.
- Bastian-Jordan M. Magnetic resonance imaging of the prostate and targeted biopsy, comparison of PIRADS and Gleason grading. *J Med Imaging Radiat Oncol.* 2018;62:183-187.
- Sathianathan NJ, Omer A, Harriss E, et al. Negative predictive value of multiparametric magnetic resonance imaging in the detection of clinically significant prostate cancer in the prostate imaging reporting and data system era: a systematic review and meta-analysis. *Eur Urol.* 2020;78:402-414.
- Ahmed HU, El-Shater Bosaily A, Brown LC, et al. Diagnostic accuracy of multi-parametric MRI and TRUS biopsy in prostate cancer (PROMIS): a paired validating confirmatory study. *Lancet.* 2017;389:815-822.
- Aihara M, Wheeler TM, Ohori M, Scardino PT. Heterogeneity of prostate cancer in radical prostatectomy specimens. *Urology.* 1994;43:60-66.
- Wei L, Wang J, Lampert E, et al. Intratumoral and Intertumoral genomic heterogeneity of multifocal localized prostate cancer impacts molecular classifications and genomic prognosticators. *Eur Urol.* 2017;71:183-192.
- Woodcock DJ, Riabchenko E, Taavitsainen S, et al. Prostate cancer evolution from multilineage primary to single lineage metastases with implications for liquid biopsy. *Nat Commun.* 2020;11:5070.
- Norris JM, Simpson BS, Parry MA, et al. Genetic landscape of prostate cancer conspicuity on multiparametric magnetic resonance imaging: a systematic review and bioinformatic analysis. *Eur Urol Open Sci.* 2020;20:37-47.
- Norris JM, Carmona Echeverria LM, Bott SRJ, et al. What type of prostate cancer is systematically overlooked by multiparametric magnetic resonance imaging? An analysis from the PROMIS cohort. *Eur Urol.* 2020;78:163-170.
- Sandeman K, Eineluoto JT, Pohjonen J, et al. Prostate MRI added to CAPRA, MSKCC and Partin cancer nomograms significantly enhances the prediction of adverse findings and biochemical recurrence after radical prostatectomy. *PLoS One.* 2020;15:e0235779.
- Lehto TK, Sturenberg C, Malen A, et al. Transcript analysis of commercial prostate cancer risk stratification panels in hard-to-predict grade group 2-4 prostate cancers. *Prostate.* 2021;81:368-376.
- Bankhead P, Loughrey MB, Fernandez JA, et al. QuPath: open source software for digital pathology image analysis. *Sci Rep.* 2017;7:16878.
- Truong M, Hollenberg G, Weinberg E, Messing EM, Miyamoto H, Frye TP. Impact of Gleason subtype on prostate cancer detection using multiparametric magnetic resonance imaging: correlation with final histopathology. *J Urol.* 2017;198:316-321.
- Mikoshi A, Miyai K, Hamabe F, et al. MRI-detectability and histological factors of prostate cancer including intraductal carcinoma and cribriform pattern. *Prostate.* 2022;82:452-463.
- Miyai K, Mikoshi A, Hamabe F, et al. Histological differences in cancer cells, stroma, and luminal spaces strongly correlate with in vivo MRI-detectability of prostate cancer. *Mod Pathol.* 2019;32:1536-1543.
- Rosenkrantz AB, Triolo MJ, Melamed J, Rusinek H, Taneja SS, Deng FM. Whole-lesion apparent diffusion coefficient metrics as a marker of percentage Gleason 4 component within Gleason 7 prostate cancer at radical prostatectomy. *J Magn Reson Imaging.* 2015;41:708-714.
- Olivier J, Li W, Nieboer D, et al. Prostate cancer patients under active surveillance with a suspicious magnetic resonance imaging finding are at increased risk of needing treatment: results of the Movember Foundation's global action plan prostate cancer active surveillance (GAP3) consortium. *Eur Urol Open Sci.* 2022;35:59-67.
- Huebner NA, Korn S, Resch I, et al. Visibility of significant prostate cancer on multiparametric magnetic resonance imaging (MRI)-do we still need contrast media? *Eur Radiol.* 2021;31:3754-3764.
- Kuhlmann PK, Chen M, Luu M, et al. Patient- and tumor-level risk factors for MRI-invisible prostate cancer. *Prostate Cancer Prostatic Dis.* 2021;24:794-801.
- Chatterjee A, Watson G, Myint E, Sved P, McEntee M, Bourne R. Changes in epithelium, stroma, and lumen space correlate more strongly with Gleason pattern and are stronger predictors of prostate ADC changes than cellularity metrics. *Radiology.* 2015;277:751-762.
- Kobus T, van der Laak JA, Maas MC, et al. Contribution of histopathologic tissue composition to quantitative MR spectroscopy and diffusion-weighted imaging of the prostate. *Radiology.* 2016;278:801-811.
- Kwak JT, Sankineni S, Xu S, et al. Prostate cancer: a correlative study of multiparametric MR imaging and digital histopathology. *Radiology.* 2017;285:147-156.
- Schieda N, Coffey N, Gulavita P, Al-Dandan O, Shabana W, Flood TA. Prostatic ductal adenocarcinoma: an aggressive tumour variant unrecognized on T2 weighted magnetic resonance imaging (MRI). *Eur Radiol.* 2014;24:1349-1356.
- Prendeville S, Gertner M, Maganti M, et al. Role of magnetic resonance imaging targeted biopsy in detection of prostate cancer harboring adverse pathological features of intraductal carcinoma and invasive cribriform carcinoma. *J Urol.* 2018;200:104-113.
- Currin S, Flood TA, Krishna S, Ansari A, McInnes MDF, Schieda N. Intraductal carcinoma of the prostate (IDC-P) lowers apparent diffusion coefficient (ADC) values among intermediate risk prostate cancers. *J Magn Reson Imaging.* 2019;50:279-287.
- Li P, You S, Nguyen C, et al. Genes involved in prostate cancer progression determine MRI visibility. *Theranostics.* 2018;8:1752-1765.
- Switlyk MD, Salberg UB, Geier OM, et al. PTEN expression in prostate cancer: relationship with clinicopathologic features and multiparametric MRI findings. *AJR Am J Roentgenol.* 2019;212:1-9.
- McCann SM, Jiang Y, Fan X, et al. Quantitative multiparametric MRI features and PTEN expression of peripheral zone prostate cancer: a pilot study. *AJR Am J Roentgenol.* 2016;206:559-565.
- Qiu X, Boufaiad N, Hallal T, et al. MYC drives aggressive prostate cancer by disrupting transcriptional pause release at androgen receptor targets. *Nat Commun.* 2022;13:2559.

36. Clark A, Burtleson M. SPOP and cancer: a systematic review. *Am J Cancer Res*. 2020;10:704-726.
37. Ju LG, Zhu Y, Long QY, et al. SPOP suppresses prostate cancer through regulation of CYCLIN E1 stability. *Cell Death Differ*. 2019;26:1156-1168.
38. Erickson A, He M, Berglund E, et al. Spatially resolved clonal copy number alterations in benign and malignant tissue. *Nature*. 2022;608:360-367.
39. Sabouri S, Chang SD, Savdie R, et al. Luminal water imaging: a new MR imaging T2 mapping technique for prostate cancer diagnosis. *Radiology*. 2017;284:451-459.
40. White NS, Leergaard TB, D'Arceuil H, Bjaalie JG, Dale AM. Probing tissue microstructure with restriction spectrum imaging: histological and theoretical validation. *Hum Brain Mapp*. 2013;34:327-346.
41. Panagiotaki E, Walker-Samuel S, Siow B, et al. Noninvasive quantification of solid tumor microstructure using VERDICT MRI. *Cancer Res*. 2014;74:1902-1912.
42. Rannikko A, Leht M, Mirtti T, et al. Population-based randomized trial of screening for clinically significant prostate cancer ProScreen: a pilot study. *BJU Int*. 2022;130:193-199.

SUPPORTING INFORMATION

Additional supporting information can be found online in the Supporting Information section at the end of this article.

How to cite this article: Lehto T-PK, Pylväläinen J, Sandeman K, et al. Histomic and transcriptomic features of MRI-visible and invisible clinically significant prostate cancers are associated with prognosis. *Int J Cancer*. 2024;154(5):926-939. doi:[10.1002/ijc.34743](https://doi.org/10.1002/ijc.34743)